

Observation of tropical rain forest trees by airborne high-resolution interferometric radar¹

Dirk H. Hoekman and Chris Varekamp
Wageningen University

Dept. of Environmental Sciences, Nieuwe Kanaal 11, 6709 PA Wageningen, The Netherlands
tel:+31-317-482894, fax:+31-317-484885,
email: dirk.hoekman@users.whh.wau.nl

Abstract

The INDREX campaign was executed in Indonesia to study the potential of high-resolution interferometric airborne radar in support of sustainable tropical forest management. Severe cloud cover limits the use of aerial photography which is currently applied on a routine basis to extract information at the tree level. Interferometric radar images may be a viable alternative once radar imaging at the tree level is sufficiently understood. It is shown that interferometric height images can contain large height and displacement errors for individual trees but that this problem can be solved to a large extent using models for the vertical distribution of backscatter intensity and an extension of the Van Cittert-Zernike theorem. The predicted loss of coherence in lay-over regions of emergent trees is shown to be in good agreement with the loss of coherence as observed in the high resolution radar data (Pearson correlation coefficient = 0.94). Several correction methods for height and displacement errors are proposed. It is shown that a simple approach already gives a good correction. Semi-empirical correction models, which can be calibrated for forest structure, perform even better.

1 Introduction

To enforce national legislation for sustainable forest management or to verify implementation of guidelines for sustainable forest management as proposed by the International Tropical Timber Organisation (ITTO), information on terrain, forest and tree characteristics is needed. Among others, systems should be available to monitor logging activities and to detect illegal logging, allowing timely action to be taken. Because cloud cover severely limits the application of aerial photography (Gastellu-Etchegorry, 1988), the use of airborne radar is proposed as an appropriate alternative.

To study the potential of radar the Indonesian Radar Experiment (INDREX) campaign was executed in Indonesia in 1996 under the auspices of the Indonesian Ministry of Forestry (MOF) and the European Space Agency (ESA). The Dornier SAR system (Fallor and Meier, 1995) collected data in several modi over Dipterocarp rain forest test sites in the provinces of East-Kalimantan and Jambi. In the same period aerial photographs were acquired and ground observations were made. In this paper results of high-resolution (1.5 m) C-band interferometric SAR data of two of the East-

Kalimantan test sites (sites A and C) are discussed. These particular test sites include the Wanariset research forest, the ITTO plot for forest rehabilitation and the ITCI concession (Attema *et al.*, 1996).

Parameters such as tree position, tree crown dimensions, canopy cover and terrain slope angle, and the location of skid trails and logging roads, are of particular interest. In principle such information can be retrieved on a routine basis over large areas from aerial photographs. Repetitive observation would allow assessment of logging intensity, erosion and fire susceptibility, verification of reforestation obligations, etc. However, cloud cover too often prevents timely observation.

Radar does not have this limitation. Moreover, images of short-wave high-resolution radar, in principle, may give sufficient information. Since other physical mechanisms underlie radar imaging, radar images can not be treated in the same way as aerial photographs. Notably effects of 'radar shadow' and 'lay-over' should be handled with care. Lay-over, for example, occurs where two tree crowns with different heights are located at the same range distance (see also figure 1). In non-interferometric radar images these two tree crowns will be imaged on top of each other, without being able to detect such a situation. In interferometric images this situation can be detected through the measurement of phase coherence. In tropical forests height differences between individual trees can be substantial and are common. Emergent trees in primary and logged-over forests can reach more than 10 m above other upper canopy trees. The same is true for secondary forest, which often comprises remnants of the former primary forest.

In theory the problem of lay-over may be solved to a large extent by making use of the observed interferometric phase coherence. Loss of coherence is indicative for lay-over and can be modelled as a function of vegetation height differences. The larger the height differences in a certain range cell the lower the observed coherence. This effect has been termed 'geometric decorrelation' (Rodriguez and Martin, 1992: p.148) or 'spatial baseline decorrelation' (Zebker and Villasenor, 1992). Expressions for the complex degree of coherence as a function of vegetation height have been given in Rodriguez and Martin (1992) and Hagberg *et al.* (1995: P.331). The authors Rodriguez and Martin (1992) note that the geometric part of the coherence is an extension of the Van Cittert-Zernike

¹ Proc. INDREX Final results workshop, ESTEC 9 Nov. 1999 & Jakarta 30 Nov. 1999: ESA SP-489, Nov. 2000, p 47-56

theorem (Van Cittert, 1939; Zernike, 1938) from two to three dimensions. The equivalence of InSAR with Δk -radar is treated in Sarabandi (1997), thus allowing the use of ground-based scatterometers for detailed experiments. To our knowledge, results from such ground experiments have not yet been published. Detailed modelling and validation for a homogeneous vegetation layer has been done in Treuhaft *et al.* (1996) using the TOPSAR instrument.

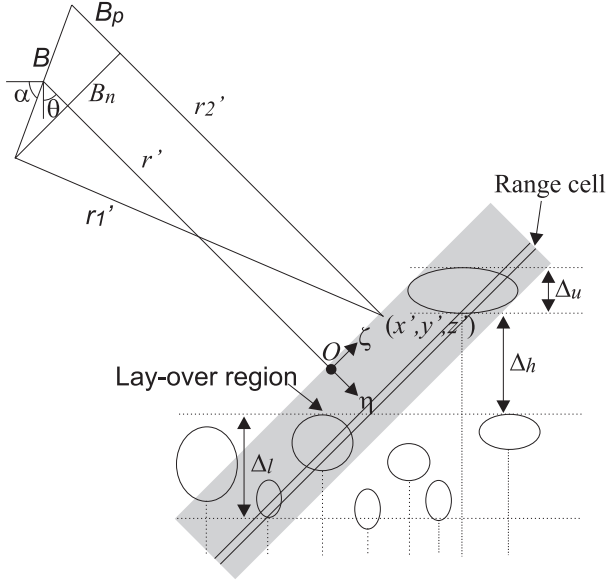


Figure 1. Lay-over in tropical rain forest. The antenna positions are numbered as 1 and 2 and are separated by the baseline distance B . A local coordinate system (η, ζ) has been defined with the origin halfway the line connecting two effective scattering layers. The thickness of the upper and lower effective scattering layers are indicated by Δ_u and Δ_l . Δ_h is the distance between these layers.

This paper concentrates on the lay-over problem. The observed coherence as found for emergent trees is compared with predictions using a simple model for the phase coherence. One can expect that both the three-dimensional shape of the tree crown and attenuation effects inside the tree crown will influence the phase coherence. Both these effects are ignored in this paper and are treated in a next paper. The first reason to do so is that most tropical trees have crowns with a rather irregular and open branch structure (see figure 6). Scattering will therefore originate from all over the crown volume and attenuation is a complicated function of crown shape and scatterer parameters. Secondly, the number of parameters in the model should be kept small to allow for inversion.

Also the effect of the trunk-ground interaction has been ignored. This effect may be relevant in some forest types, especially for HH-polarisation at small incidence angles (Sarabandi and Lin, 1997). It has been one of the considerations to conduct this experiment at large incidence angles and at VV-polarisation. Moreover, most trunks are located on slopes, the crown coverage is

very high and a shrub layer is usually present, which further diminishes the relevance of this term.

It will be shown that this simplified approach allows for 3-D position correction of the highest tree when two crowns with considerable height difference are mapped into the same resolution cell. Application of this simple model may be basic to the development of inversion algorithms for automated production of 3-D tree maps.

2 Theory

2.1 Coherence model

The following derivation is similar to the one given in Hagberg *et al.* (1995: p.331). Radiation extinction as well as backscattering from the ground and from stems are ignored for reasons pointed out in the introduction. The complex cross-correlation can now be written as (Ishimaru, 1978: p.87; Goodman, 1985)

$$\langle E_1(x_1, r_1) E_2^*(x_2, r_2) \rangle = K \int_V \sigma_v(x', y', z') \cdot e^{i2k(r_1'(y', z') - r_2'(y', z'))} \cdot W(x_1 - x', r_1 - r_1'(y', z')) W^*(x_2 - x', r_2 - r_2'(y', z')) dV' \quad (1)$$

where

- E_1, E_2 = electric field strengths received by antennas 1 and 2
- (x_1, r_1) = image coordinates of image 1
- (x_2, r_2) = image coordinates of image 2
- K = radar dependent parameter
- k = wave number, $2\pi / \lambda$ (m^{-1})
- λ = wavelength (m)
- σ_v = volume backscatter coefficient ($m^2 m^{-3}$)
- W = radar impulse response function
- V = range cell volume
- dV' = elementary volume $dx'dy'dz'$

The unprimed coordinates correspond to a reference point for the impulse response whereas the primed coordinates correspond to the scatter location. A simplified interferometric SAR geometry is shown in figure 1. A local ζ -axis has been introduced at distance r' and parallel to the 'effective baseline component' indicated with B_n . Following the paraxial approximation (Goodman, 1985: p.209) $B_n = B \cos(\theta - \alpha)$. Finally, an axis $\eta = r_1 - r_1(y', z')$ is introduced orthogonal to the ζ -axis. The ζ' -axis parallel to the x' -axis completes the new coordinate system. Assuming perfect registration of image 1 and image 2, the coherence magnitude can be expressed as the product of 'noise' coherence, volume coherence and slant range coherence magnitudes (Zebker and Villasenor, 1992; Askne *et al.*, 1997)

$$|\rho| = \frac{\iint \sigma_v(z') |W(\xi', \eta')|^2 d\xi' d\eta'}{\iint \sigma_v(z') |W(\xi', \eta')|^2 d\xi' d\eta' + |n|^2} \quad (2)$$

$$= \frac{\left| \int \sigma_v(z') e^{i \frac{2kB_n}{R \sin \theta} z'} dz' \right| \left| \iint |W(\xi', \eta')|^2 e^{i \frac{2kB_n}{R \tan \theta} \eta'} d\xi' d\eta' \right|}{\int \sigma_v(z') dz' \iint |W(\xi', \eta')|^2 d\xi' d\eta'}$$

$$= |\rho|_{noise} |\rho|_{volume} |\rho|_{slanrange}$$

where n represents thermal noise, and $|\rho|_{noise}$ depends only on the signal to noise ratio (SNR)

$$|\rho|_{noise} = \frac{SNR}{SNR + 1} \quad (3)$$

In the next sections it is assumed $|\rho|_{noise} = |\rho|_{slanrange} = 1$. The validity of this approximation will be shown later in section 3. Note that equations 1 and 2 contain an additional factor 2 in the complex exponentials due to the ping-pong mode that was deployed by the Dornier SAR instrument for the acquisitions of the images analysed in this paper.

2.2 Models for $\sigma_v(z')$

Now consider a lay-over situation where a tall tree extends above the other trees (figure 2). Two effective scattering layers with thickness Δ_l and Δ_u separated by distance Δ_h are shown. The upper layer with thickness Δ_u represents a single emergent tree crown whereas the lower layer represents the lay-over region with thickness Δ_l . The volume backscattering coefficient is assumed to be only a function of

$$\sigma_v(z') = \sigma_{v,u}(z') + \sigma_{v,l}(z') \quad (4)$$

with $\sigma_{v,u}(z')$ and $\sigma_{v,l}(z')$ the volume backscattering coefficients ($m^2 m^{-3}$) for the upper and lower effective scattering layers, respectively. It seems reasonable to assume that the backscatter coefficient σ^0 ($m^2 m^{-2}$) for an emergent tree (in isolation, i.e. without its lay-over region) approximates the backscatter coefficient for the forest on average. Because emergent tree crowns are imaged as lay-over regions, the backscatter coefficient is expected to be about twice as high due to the contribution of the lower vegetation layer. This was verified (using a procedure explained in more detail in section 3) by comparing the average intensity of a large image subset of 1000 range by 2000 azimuth pixels to the average intensity of a large number of lay-over regions of emergent trees. The average image intensity for the lay-over regions of emergent trees was found to be 1.80 times the average image intensity of the large

image subset. Consequently, it may be assumed that on average σ_u^0 is slightly lower than σ_l^0 with

$$\sigma_u^0 = \int \sigma_{v,u}(z') dz' \quad \text{and} \quad \sigma_l^0 = \int \sigma_{v,l}(z') dz'. \quad (5)$$

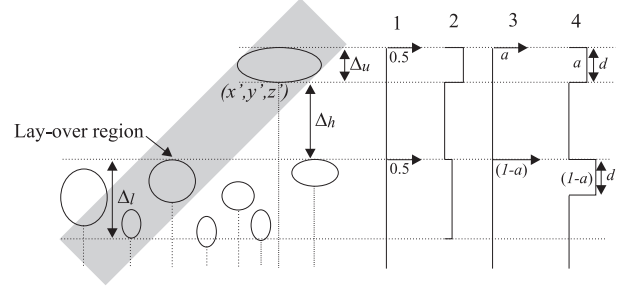


Figure 2. Schematic illustration of effective scattering layers together with a schematic representation of the four functions used for the vertical distribution of the volume backscatter coefficient $\sigma_v(z')$. Function 1 (equation 7): Two infinitesimal small layers of equal backscatter strength. Function 2 (equation 11): Two layers of equal backscatter strength. Function 3 (equation 13): Two infinitesimal small layers with different backscatter strength (fractions a and $(1-a)$). Function 4 (equation 14): Two layers of different backscatter strength (fractions a and $(1-a)$), but with equal thickness d .

The coherence was modelled using four different functions for $\sigma_v(z')$. The first function for $\sigma_v(z')$ simply assumes two scattering points (figure 2)

$$\sigma_v(z') = \sigma_u^0 \delta\left(z' - \frac{\Delta_h + \Delta_u}{2}\right) + \sigma_l^0 \delta\left(z' + \frac{\Delta_h + \Delta_u}{2}\right) \quad (6)$$

with $\delta(z')$ the Dirac delta function (m^{-1}). Both scattering points lie at the top of their respective layer which means that the points are separated by a distance $\Delta_h + \Delta_u$. Next, equal scattering of both points is assumed: $\sigma_u^0 = \sigma_l^0$. Using (6) in (2)

$$\rho = \rho_{volume} = e^{-i2kB_p} \left(\frac{e^{i\beta\left(\frac{\Delta_h + \Delta_u}{2}\right)} + e^{-i\beta\left(\frac{\Delta_h + \Delta_u}{2}\right)}}{2} \right) \quad (7)$$

with

$$\beta = \frac{2kB_n}{r \sin \theta}. \quad (8)$$

It follows that

$$|\rho| = \cos\left(\beta\left(\frac{\Delta_h + \Delta_u}{2}\right)\right), \quad (9)$$

which is illustrated in figure 3 where $|\rho|$ is shown as a function of $\Delta_h + \Delta_u$. The second function for $\sigma_v(z')$ assumes a rectangular function for $\sigma_{v,u}(z')$ and $\sigma_{v,l}(z')$ and equal scattering of both layers, i.e. $\sigma_u^0 = \sigma_l^0$ (figure 2):

$$\sigma_v(z') = \sigma_u^0 \chi\left(\frac{\Delta_h}{2}, \frac{\Delta_h}{2} + \Delta_u\right) + \sigma_l^0 \chi\left(-\frac{\Delta_h}{2} - \Delta_l, -\frac{\Delta_h}{2}\right) \quad (10)$$

with

$$\chi(a, b) = \begin{cases} \frac{1}{b-a} & (a < z' < b) \\ 0 & \text{otherwise} \end{cases}$$

And ρ follows as

$$\rho = \frac{e^{-i2kB_p}}{i2\beta} \left[\frac{1}{\Delta_u} \left(e^{i\beta\left(\frac{\Delta_h}{2} + \Delta_u\right)} - e^{i\beta\left(\frac{\Delta_h}{2}\right)} \right) + \frac{1}{\Delta_l} \left(e^{i\beta\left(-\frac{\Delta_h}{2}\right)} - e^{i\beta\left(-\frac{\Delta_h}{2} - \Delta_l\right)} \right) \right] \quad (11)$$

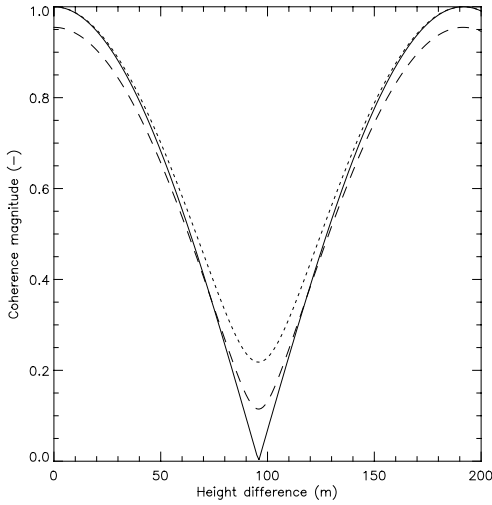


Figure 3. Plot of $|\rho|$ as a function of height difference $\Delta_h + \Delta_u$: For the symmetric delta function (solid line), for the asymmetric delta function (short dash) with $a=0.629$ and for the asymmetric rectangular function (long dash) and with $a=0.56$ and $d=32$ m. The following system dependent variables were used: $\theta = 54.7$ deg, $r=5592$ m, $B_n=0.674$ m.

As a more general case, it can be assumed that the backscatter of the upper layer differs from the lower layer. When the fractions a and b are introduced as (also see figure 2):

$$a = \frac{\sigma_u^0}{\sigma_u^0 + \sigma_l^0} \quad \text{and} \quad b = \frac{\sigma_l^0}{\sigma_u^0 + \sigma_l^0} \quad (12)$$

then, equations 7 and 11 can be rewritten, respectively, as

$$\rho = e^{-i2kB_p} \left[a e^{i\beta\left(\frac{\Delta_h + \Delta_u}{2}\right)} + (1-a) e^{-i\beta\left(\frac{\Delta_h + \Delta_u}{2}\right)} \right] \quad (13)$$

and

$$\rho = \frac{e^{-i2kB_p}}{i\beta} \left[\frac{a}{\Delta_u} \left(e^{i\beta\left(\frac{\Delta_h}{2} + \Delta_u\right)} - e^{i\beta\left(\frac{\Delta_h}{2}\right)} \right) + \frac{(1-a)}{\Delta_l} \left(e^{i\beta\left(-\frac{\Delta_h}{2}\right)} - e^{i\beta\left(-\frac{\Delta_h}{2} - \Delta_l\right)} \right) \right] \quad (14)$$

In the following these coherence models will be referred to as: the symmetric delta function (equation 7), the symmetric rectangular function (equation 11), the asymmetric delta function (equation 13) and the asymmetric rectangular function (equation 14).

2.3 Bias of emergent tree crown position reconstruction

In the very simple case of the symmetric delta function for $\sigma_v(z')$, the coherence magnitude is the absolute value of a cosine function of the height difference between the top of the emergent tree and the top of the canopy in the lay-over region (equation 9 and figure 3). The solution to equation 9 is unique when

$$0 \leq \beta \left(\frac{\Delta_h + \Delta_u}{2} \right) \leq \frac{\pi}{2} \quad (15)$$

For the system parameters mentioned in the caption of figure 3 the corresponding height difference range is $0 \leq \Delta_h + \Delta_u \leq 94.8$ m. Under the assumption that the position of the scattering phase centre is halfway the true position of the tree top and the true position of its lay-over region, for this specific range of height differences, the observed crown coordinates (y, z) can be corrected using equation 9 as

$$y_c = y + \frac{r \cos \theta}{2kB_n} \cos^{-1} |\rho| \quad (16)$$

$$z_c = z + \frac{r \sin \theta}{2kB_n} \cos^{-1} |\rho| \quad (17)$$

In case these correction equations are applied, while the forest layers in reality are asymmetric, i.e. $a \neq b$, a bias in the position reconstruction of the emergent tree results. This bias is caused by a shift of the scattering phase centre in the direction of the layer with highest backscatter and a lower reconstruction (or correction) shift towards the upper layer (since $|\rho|$ is smaller). This bias is graphically depicted in figure 4 for both the

asymmetric delta function (equation 13) and for the asymmetric rectangular function (equation 14) with a as the asymmetry parameter. Obviously, under the assumption the forest layers can be modelled by the symmetric delta function (equation 7), the correction equations 16 and 17 perform well in case there is no lay-over ($a=1$), and in cases where there is lay-over and the backscatter of the upper and lower layers are equal ($a=0.5$). In the latter case a large error is made when no correction is applied. For all other cases a bias results, which, for large values of a , in absolute sense even exceeds the error resulting from not applying a correction. Under the assumption that the forest layers can be modelled by a symmetric rectangular function, representing layers of 5 m thickness in this example, and correction equations 16 and 17 are applied, different biases result (see also figure 4). In general, it can be stated that the bias depends on the shapes of both upper and lower layer and that good height corrections for individual trees are only possible when these shapes are known *a priori* for each tree. In practical situations it may be feasible to adopt an 'efficient average' shape, resulting in 'optimised' correction equations.

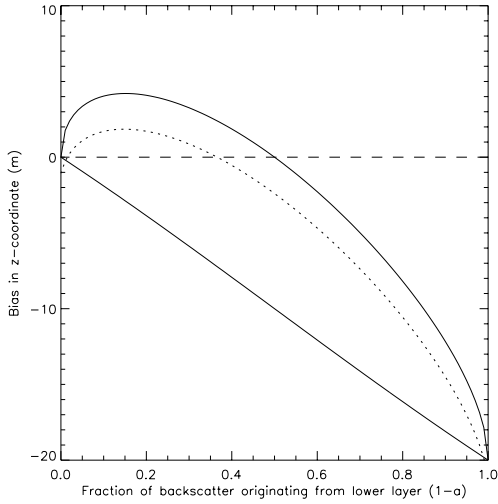


Figure 4. The bias as a function of the asymmetry parameter a for three cases. (a) The layers are described by an asymmetric delta function with a spacing $\Delta_h=20$ m and no correction is applied (lower solid line). (b) The layers are described by an asymmetric delta function with a spacing $\Delta_h=20$ m and a correction is applied assuming a symmetric delta function is valid (upper solid line). (c) The layers are described with by an asymmetric rectangular shape with a spacing $\Delta_h=15$ m and layer thicknesses $\Delta_u=\Delta_l=5$ m and a correction is applied assuming a symmetric delta function is valid (dotted line).

2.4 Calibration of the correction equations

Suppose that on average tree positions are best corrected by assuming an asymmetric Dirac delta function. In that case, like correction equations 16 and 17 follow from equation 12, alternative correction equations follow

from equation 13 by replacing the term $\cos^{-1}(|\rho|)$ in 16 and 17 with:

$$\sin^{-1} \left(\sqrt{\frac{1-|\rho|^2}{(4a-4a^2)}} \right) - \tan^{-1} \left((2a-1) \tan \left(\sin^{-1} \sqrt{\frac{1-|\rho|^2}{(4a-4a^2)}} \right) \right) \quad (18)$$

In case a set of data with real tree heights and corrected interferometric tree heights is available the value of the asymmetry parameter a could be tuned to remove the bias, or to minimise the Mean Square Error (*MSE*), on average.

Of course even more complicated correction equations may be developed, e.g. by assuming an asymmetric rectangular function with fixed thickness d representing the average layer thickness. In this case two parameter values: a and d , are fitted empirically. Now alternative correction equations follow from equation 14 by replacing the term $\cos^{-1}(|\rho|)$ in 17 and 17 with:

$$x - \tan^{-1} \left[\frac{(1-2a)[\cos(x+\beta d) - \cos(x)]}{[\sin(x+\beta d) - \sin(x)]} \right] + \beta d \quad (19)$$

where

$$x = \sin^{-1} \sqrt{\frac{\beta^2 d^2 |\rho|^2 - 2(1 - \cos(\beta d))}{2(4a^2 - 4a)(1 - \cos(\beta d))}} - 0.5\beta d .$$

The merit of such a semi-empirical approach is that bias removal may be optimised better, while the values of such parameters may be related to forest structure types. This will be discussed in section 4.

3 Experiment

3.1 InSAR data

Relevant Dornier SAR sensor parameters and image acquisition parameters for tracks Kal.17A, Kal.18A and Kal.19C (Attema *et al.*, 1996) are listed in table 1. The basic SAR data types used were the multilook (L -look) average intensity of the first antenna, and the complex interferogram $\hat{\rho}$ given by

$$|E_1|^2 = \frac{1}{L} \sum_{l=1}^L |E_{1,l}|^2 \quad (20)$$

and

$$\hat{\rho} = \frac{\sum_{l=1}^L E_{1,l} E_{2,l}^*}{\sqrt{\sum_{l=1}^L |E_{1,l}|^2 \sum_{l=1}^L |E_{2,l}|^2}} \quad (21)$$

where L is the number of looks per pixel. The z -coordinate image was calculated from the phase difference $\arg(\hat{\rho})$ after phase unwrapping and using the parameters in table 1. Figure 5 shows slant range images of the z -coordinate, the backscatter amplitude and the coherence magnitude for a subset of track Kal.19C. Labelled polygons roughly indicate the positions of the crowns of large trees which were selected during fieldwork.

Table 1. Dornier SAR sensor and image parameters for tracks Kal.17A, Kal.18A and Kal.19C of the INDREX 1996 campaign.

	Kal.17A	Kal.18A	Kal.19C
centre frequency (GHz)		5.3	
Bandwidth (MHz)		100	
Polarisation		VV	
operating altitude (m)	3238	3243	3228
Horizontal baseline component (m)		0.115	
vertical baseline component (m)		0.744	
swath width (m)		2000	
incidence angle range (deg)		48 - 63	
number of independent looks		4	
range resolution (m)	1.75	1.75	1.75
azimuth resolution (m)	0.34	0.47	0.34
range pixel spacing (m)	1.25	1.25	1.25
azimuth pixel spacing (m)	1.37	1.89	1.36

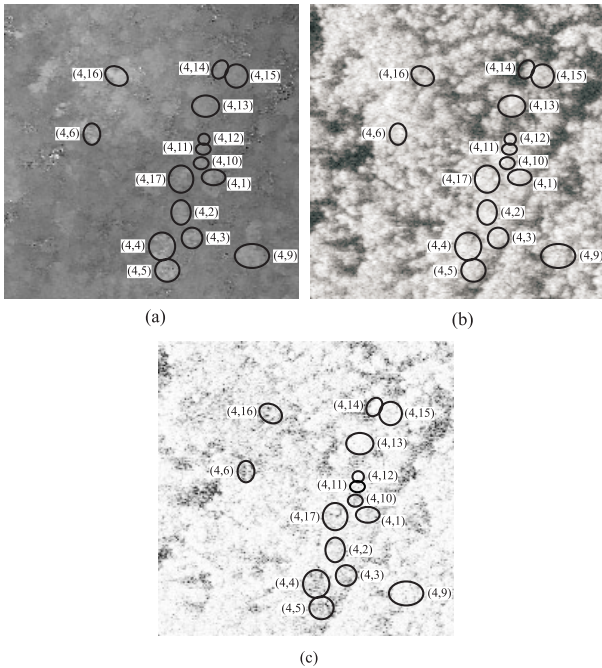


Figure 5. Subset of 200×200 pixels of slant range radar data covering study plot 4 which is located in the ITTO plot. Images of (a) z -coordinate, (b) backscatter intensity and (c) coherence magnitude are shown. The z -coordinate is scaled between 75 m and 200 m. The backscatter intensity has a range of 41.8 dB. The coherence magnitude is scaled between 0.8 and 1.

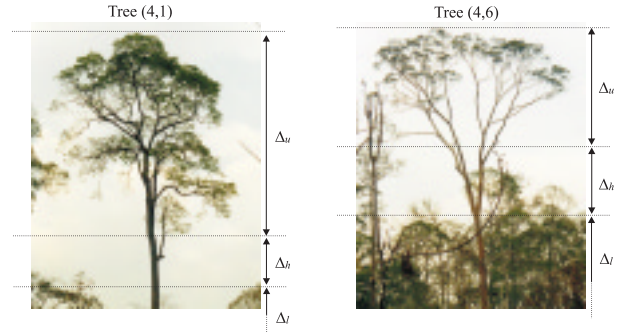


Figure 6. Two photographs of typical trees occurring in the radar data in figure 5. The dimensions given in the photographs are only indicative of the real measurements.

3.2 Field measurements

In situ measurements were made of large individual trees in several study sites in East-Kalimantan. Tree positions were measured relative to other trees or relative to known points on a road. For each tree, the total tree height, tree crown dimensions, the height of the tree base relative to all trees in the same study plot, and the characteristics of the terrain and vegetation in the lay-over region were measured. In addition it was noted whether the vegetation in the lay-over region was in the radar shadow of trees closer to the radar (see figure 7). Also each tree crown was photographed from different directions. For these trees Δ_l , Δ_u and Δ_h were determined from the field measurements. A total of 42 trees were selected, for which the lay-over region was not shadowed by trees closer to the radar. The values are listed in table 2. It can be seen from table 1 and table 2 that the resolution is fine compared to the layer dimensions Δ_l and Δ_u separated by distance Δ_h and Δ_l and the layer separation Δ_h . The slant range coherence magnitude $|\rho|_{slanrange}$ will decrease as a function of scattering layer thickness. Even for a scattering layer with a thickness of 50 m $|\rho|_{slanrange} = 0.996$, which is still very close to 1. Therefore slant range decorrelation will be ignored. Decorrelation due to noise is also a small effect. Using the intensity of a smooth water surface in the far range and the intensity of forest vegetation a SNR of 25.92 dB is found. The $|\rho|_{noise}$ follows from equation 2 and equals 0.997. Therefore noise decorrelation will be ignored. Note that the decorrelation due to these two effects ($1 - |\rho|_{noise} |\rho|_{slanrange}$) is 0.007 which is still minor compared to the smallest total decorrelation found for the trees measured (see table 2).

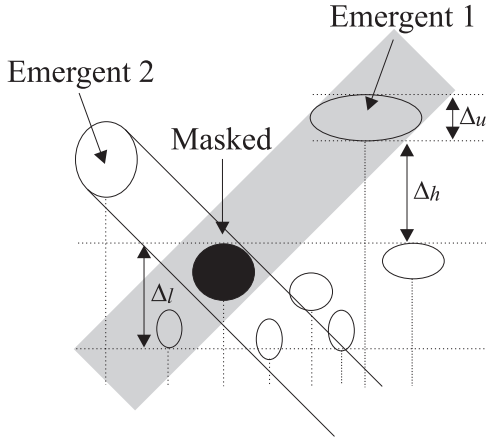


Figure 7. Shadowing of the lay-over region.

Table 2. Measurement of thickness of lower layer (Δ_l), thickness of upper layer (Δ_u), layer separation (Δ_h), number of crown pixels (N) and coherence magnitude ($|\rho|$).

Crown	Δ_l	Δ_u	Δ_h	N	$ \rho $
Track Kal.19C					
2.1	2	12.5	10	55	0.9567
3.1	10	13	15	43	0.9213
3.2	10	10	13	58	0.9263
3.3	10	14	11	183	0.9123
4.1	5	18	13	87	0.8634
4.2	5	10.5	16	131	0.8724
4.3	5	11	25	95	0.8029
4.4	5	18	29	192	0.7590
4.5	5	16	27.5	194	0.7689
4.6	5	19	29	168	0.7203
4.9	7	12	17.5	246	0.8938
4.10	5	15	21.5	37	0.8505
4.11	10	12	11	29	0.9132
4.12	10	19.5	-4	77	0.9434
4.13	10	19	3.5	128	0.9548
4.14	10	13	7	86	0.9148
4.15	10	12	10	140	0.9248
4.16	10	26.5	9	105	0.8080
4.17	5	18.75	16	101	0.8610
6.1	5	17.75	-4	176	0.9287
6.2	5	22	21	127	0.8521
6.3	5	19	14	134	0.8504
6.4	5	28	1	170	0.9221
6.5	5	14	17	107	0.9177
Track Kal.17A					
17.1	9.1	25	16.7	100	0.7935
17.2	3.3	7	20.8	39	0.9240
17.3	6	16	21	105	0.8070
17.4	12	27	22	222	0.7245
17.8	2	20	40	77	0.5735
17.9	0.5	20	43.5	138	0.6481
17.35	15.7	22	6.2	139	0.9080
17.101	15	39.6	-2	267	0.6966
17.102	10	31	31	149	0.7013
Track Kal.18A					
18.1	25.3	25	2.7	129	0.7744
18.2	6.4	7	15.3	23	0.8346
18.3	21.2	16	10	71	0.7526
18.4	15	27	23	117	0.5987
18.7	40.2	20	0.1	116	0.7534
18.11	5	22	19	77	0.6507
18.35	17.3	22	16.6	79	0.7319
18.101	5	39.6	18	226	0.6113
18.102	10	31	31	162	0.6390

3.3 Crown identification and data extraction

The 42 tree crowns were identified in the radar images with the help of tree position drawings and tree crown photographs. The next step consisted of careful digitisation of the tree crown. This digitisation step was done in a median filtered version of the z -coordinate image. A 3×3 window was used for filtering. Figure 8 shows for crowns 4.1 and 4.6 the intensity image, z -coordinate image, coherence magnitude image, a median filtered z -coordinate image, and the extracted pixel regions. The grey region contains the tree crown pixels. The white region contains neighbouring pixels covering adjacent lower vegetation. The average height of these neighbouring pixels is assumed to be representative of the height of the lower layer in the lay-over region. Figure 9 illustrates the two regions. For each crown region the average z -coordinate (using the non-filtered data) and the coherence magnitude are calculated. The coherence magnitude was estimated with

$$\rho = \frac{1}{N} \left| \sum_{j=1}^N \hat{\rho}_j \right| \quad (22)$$

where N is the number of crown pixels. For each region of neighbouring pixels the average z -coordinate is also estimated.

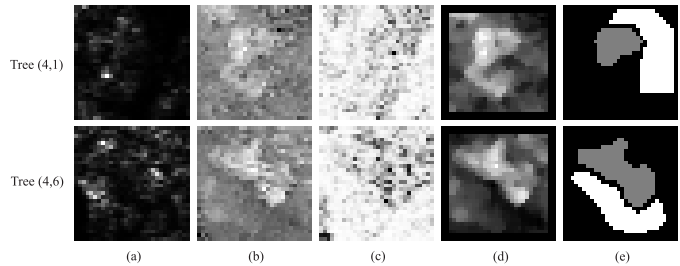


Figure 8. The intensity image, z -coordinate image, coherence magnitude image, a median filtered z -coordinate image, and the extracted pixel regions for crowns 4.1 and 4.6. The grey region contains the tree crown pixels. The white region contains neighbouring pixels covering adjacent lower vegetation.

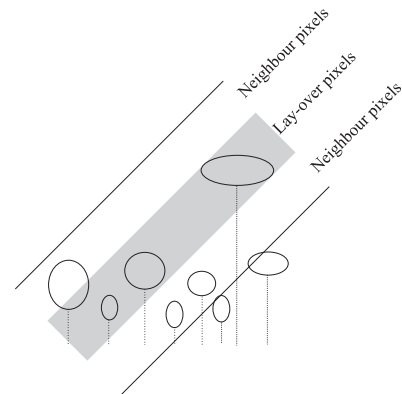


Figure 9. Illustration of pixels covering the lay-over region and neighbouring pixels covering the adjacent lower vegetation.

The coherence magnitude estimations are biased and the accuracy of these estimations depends on the sample size. Table 3 gives an indication of the bias of the estimate for 4-look data and an indication of the large sample variance of the estimate for a sample of N uncorrelated pixels for several values of $|\rho|$ according Touzi *et al.* (1999). The number of looks specified by Dornier is 5. To verify this, and to determine the effective number of independent looks, the coherence of a river water surface in the far range was measured. Its value of 0.4659 is very close to the value of 0.4571 for 4-look data, that can be computed for a completely uncorrelated surface, and much higher than the value of 0.4063 for 5-look data Touzi *et al.* (1999). Therefore, since the water surface still may show some coherence, the number of 4 can be regarded as a minimum value for the number of independent looks. By studying the image intensity of a large homogeneous rice field it could be shown that the pixels have considerable spatial correlation in range, and to a lesser extent in azimuth. As a result the number of independent pixels reduces to 38% (in the worst case) of the sample sizes indicated in table 2. In the worst case, i.e. for $|\rho| = 0.5$ and for the minimum sample size, i.e. 23, the standard deviation of the estimate can be calculated as 0.141. In practice the standard deviations are much lower, because $|\rho|$ is usually much higher and the lower values of $|\rho|$ are associated with large samples (large trees) as can be derived from this table.

Table 3. Bias and variance of the coherence magnitude estimation for several values of $|\rho|$ for 4-look data according Touzi *et al.* (1999). Note that the variance values only apply for a sufficiently large number of pixels N .

$ \rho $	bias	variance
0.5	-0.024	0.1802 / N
0.75	-0.023	0.0971 / N
0.95	-0.007	0.0181 / N
0.99	-0.002	0.0034 / N

4 Results and discussion

4.1 Coherence modelling

For the 42 selected trees the observed coherence magnitude was compared with the coherence magnitude predicted according equations 7 and 11, i.e. the symmetric delta and symmetric rectangular functions, respectively, by substituting values for Δ_l , Δ_u and Δ_h as recorded in the field. The results are shown in figures 11 and 12. Both models predict the coherence magnitude well. For the symmetric delta function the correlation between observed and predicted coherence is 0.912 and the mean error is 0.007. For the symmetric rectangular function these numbers are 0.942 and 0.042, respectively. The first function, in general, predicts values that are slightly too low for low values and slightly too high for high values of the coherence magnitude. The underlying physical cause may be that

for the high values of coherence, which relates to small values of $\Delta_u + \Delta_h$, the lower layer thickness Δ_l still may be substantial, and should not be ignored as is done when using this function. For large values of coherence the reverse may be true, i.e. the thickness of the upper layer Δ_u may be too large to be ignored. The second function, in general, predicts values that are too high for the whole range of observed coherence magnitudes. The reason may be that the upper parts of the layers scatter more than the lower parts, or that one of the two layers, i.e. either the upper or the lower layer, scatters significantly more than the other.

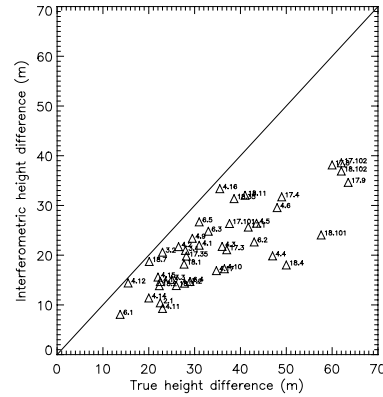


Figure 10. Interferometric height difference as a function of the true height difference.

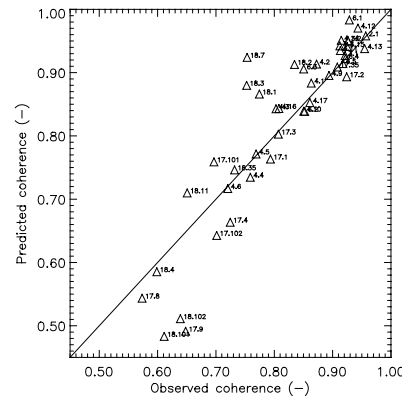


Figure 11. Coherence predicted with symmetric delta function against the observed coherence.

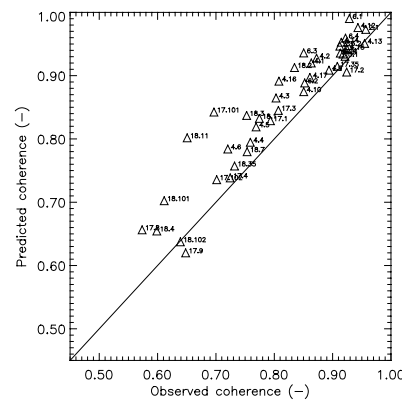


Figure 12. Coherence predicted with rectangular function against the observed coherence.

complicated structure of tropical rain forest in this way may be an oversimplification, not resulting in major additional corrections of tree crown positions.

Table 4. Bias removal: Approaches, Mean Errors (ME) and Mean Squared Errors (MSE). Minimising the MSE fits the empirical parameters of the calibration models.

Approach	ME(m)	MSE(m ²)
No correction (figure 10)	-13.17	240.14
Simple correction (eqs. 16, 17, figure 13)	5.14	62.16
Calibration model 1: $a=0.63$ (eq.13, fig 14)	0.01	43.40
Calibration model 2: $a=0.56$, $d=32$ (eq.14, fig 15)	0.48	37.94

5 Conclusions

The results show that coherence magnitudes of emergent trees can be predicted well on the basis of field observations and the use of simple models for the vertical distribution of backscatter intensity. It is also shown that in interferometric images large height and displacement errors can occur for individual emergent trees and that these errors can be corrected using these simple models. It is shown that a representation in which all backscatter is assumed to be originating from horizontal planes located at the top of the emergent tree and at the top of its lay-over region already gives a fairly good result. Further extension to horizontal layers improves the coherence magnitude modelling for individual trees. However, it seems difficult to find an 'effective' mean layer thickness, which can be used to improve correction for height and displacement errors. Apparently the structure of the tropical rain forest at the studied site is too complex to make this meaningful. Though the application of correction models is useful since they give a major reduction of the MSE, the MSE value itself should be interpreted with care. The correction applied is a correction based on the observed coherence magnitude of the emergent crown and its lay-over region. The (relative) interferometric height of the tree can only be measured relative to the (relative) interferometric height of its surroundings. Since the height of the surroundings of the lay-over region may differ from the height of the lay-over region an additional error is introduced. In other words: the expected accuracy of height correction may be larger than the value of the MSE indicates. On the other hand it should be noted that the best corrections methods are based on calibrations for which the same trees are used. Moreover, such a calibration is forest structure dependent and may not give optimal results when applied in other forest types. However, from a physical point of view, it is interesting to study the values of the parameters fitted for the calibration models since they reveal properties of the forest structure. For the set of 42 trees studied, for example, it could be concluded that slightly more backscatter originates from the emergent crown as compared to its lay-over region and that the concept of effective mean layers is hardly meaningful. The results indicated in this paper may be very useful for the development of algorithms for automated tree map production (Varekamp and Hoekman, 1999).

Further physical modelling and tree mapping developments are planned using data of a fully inventoried 7.2 ha plot, for which additional X-band data and additional C-band data with a different look direction exist. The large time elapsed between INDREX radar data collection and the various field observation periods (up to 3 years now) poses some interpretation problems. For this reason a new campaign in Kalimantan is under consideration.

Acknowledgements

We acknowledge MOFEC (formally MOF) and ESA for realisation of the INDREX campaign, Dornier Satellitensysteme GmbH for SAR data acquisition and the MOFEC-Tropenbos Kalimantan project for logistic support. The Dutch Remote Sensing Board is acknowledged for financial support. We also wish to thank Martin Vissers, Anjo de Jong and Eric van Valkengoed for assistance and ideas. Finally the anonymous reviewers are acknowledged for their valuable suggestions.

References

- Askne, J.I.H., P.B.G. Dammert, L.M.H. Ulander and G. Smith, 1997. C-Band Repeat-Pass Interferometric SAR Observation of the Forest. *IEEE Transactions on Geoscience and Remote Sensing*, 35 (1) pp. 25-35.
- Attema, E.P.W. and F.T. Ulaby, 1978. Vegetation Modelled as a Water Cloud. *Radio Science*, 13 (2) pp. 357-364.
- Cittert, P.H. Van, 1939. Kohaerenz-Probleme. *Physica*, VI (10) pp. 1129-1139.
- Faller, N.P. and E.H. Meier, 1995. First Results with the Airborne Single-Pass DO-SAR Interferometer. *IEEE Trans. Geosci. Remote Sensing*, 33 (5) pp. 1230-1237.
- Gastellu-Etchegorry, J.P., 1988. Cloud Cover Distribution in Indonesia. *International Journal of Remote Sensing*, 9 (7) pp. 1267-1276.
- Goodman, J., 1985. *Statistical Optics*. Wiley-Interscience, New York.
- Hagberg, J.O., L.M.H. Ulander and J. Askne, 1995. Repeat-Pass SAR Interferometry Over Forested Terrain. *IEEE Trans. Geosci. Remote Sensing*, 33 (2) pp. 331-340.
- Ishimaru, A., 1978. *Wave Propagation and Scattering in Random Media*, volume 1: Single Scattering and Transport Theory. Academic Press, New York.
- Rodriguez, E. and J.M. Martin, 1992. Theory and Design of Interferometric Synthetic Aperture Radars. *IEE Proceedings-F*, 139 (2) pp. 147-159.
- Sarabandi, K., 1997. Delta k-Radar Equivalent of Interferometric {SAR's}: A Theoretical Study for Determination of Vegetation Height. *IEEE Trans. Geosci. Remote Sensing*, 35 (5) pp. 1267-1276.
- Sarabandi, K. and Y-C Lin, 1997. Simulation of Interferometric SAR Response to Deciduous and Coniferous Forest Stands. *Proceedings IGARSS'97, 3-8 August 1997, Singapore*, pp. 1887-1889.
- Touzi, R., A. Lopes, J. Bruniquel and P.W. Vachon, 1999. Coherence Estimation for SAR Imagery. *IEEE Transactions on Geoscience and Remote Sensing*, 37 (1) pp. 135-149.
- Treuhaft, R.N., S.N. Madsen, M. Moghaddam and J.J. Van Zyl, 1996. Vegetation Characteristics and Underlying Topography from Interferometric Radar. *Radio Science*, 31 (6) pp. 1449-1485.
- Varekamp, C. and D.H. Hoekman, 1999. Interferometric Phase Difference Segmentation Using Parameterised Deformable Templates. *Fifth Annual Conference of the Advanced School for Computing and Imaging*, 15-17 June.
- Zebker, H.A. and J. Villasenor, 1992. Decorrelation in Interferometric Radar Echoes. *IEEE Transactions on Geoscience and Remote Sensing*, 30 (5) pp. 950-959.
- Zernike, F., 1938. The Concept of Degree of Coherence and its Applications to Optical Problems. *Physica*, V (8) pp. 785-795.

